Room temperature and narrow intersubband electroluminescence from ZnCdSe/ZnCdMgSe quantum cascade laser structures

Yu Yao,[1,a)] Adrian Alfaro-Martinez,[2,b)] Kale J. Franz,[1,c)] William O. Charles,[1,d)] Aidong Shen,[3] Maria C. Tamargo,[2] and Claire F. Gmachl[1]
[1]*Department of Electrical Engineering, Princeton University, Princeton, New Jersey 08544, USA*
[2]*Department of Chemistry, the City College of New York, New York 10031, USA*
[3]*Department of Electrical Engineering, the City College of New York, New York 10031, USA*

(Received 23 May 2011; accepted 30 June 2011; published online 29 July 2011)

We report ZnCdSe/ZnCdMgSe Quantum Cascade structures with "two-phonon" and "bound-to-continuum" active region designs. The electroluminescence shows more than 3 times higher luminescence efficiency and 40% narrower linewidth (<30 meV) than previous reports. The measured turn-on voltage matches closely the calculated value, indicating the improved electron transport characteristics in these structures. A waveguide design suitable for mode confinement in this material system is also presented, which resulted in a structure with a single narrow electroluminescence peak for all temperatures from 80 to 300 K. © *2011 American Institute of Physics*. [doi:10.1063/1.3614561]

Quantum Cascade (QC) lasers have become the most promising candidates for applications such as trace gas sensing, environmental monitoring, bio-medical sensing, and infrared counter measures because of their compactness, flexibility in emission wavelength, and high output power. Quantum Cascade lasers based on the conventional InGaAs/AlInAs material system on InP substrate have been successively improved to achieve high power and high efficiency performance above 4 μm.[1–4] However, it is more difficult to achieve high performance lasers as the wavelength becomes shorter than 4 μm due to the limited conduction band offset and the inter-valley scattering in this material system.[5] The shortest emission wavelength that has been demonstrated for continuous wave operation at room temperature so far is 3.76 μm by improving material quality and interface control in strain-balanced $In_{0.76}Ga_{0.24}As/Al_{0.74}In_{0.26}As$ QC structures.[6] In addressing this fundamental limit, other techniques are intensively investigated, such as Sb-based QC lasers[7,8] and interband cascade lasers.[9]

Besides the traditional III-V material systems, the ZnCdSe/ZnMgSe system grown lattice matched on InP substrate has been proposed as a large band-offset QC emitter alternative because the conduction band offset is estimated to be ~1.12 eV.[10] Besides, inter-valley scattering does not limit the shortest wavelength photon generation since the satellite valleys are at least 1.3 eV above the Γ valley.[11] Therefore, the II-VI material system is promising for high performance QC emitters in the 3-5 μm wavelength range and makes it in principle possible to achieve emission wavelengths as short as 1.5 μm. We have previously demonstrated electroluminescence (EL) at ~4.8 μm from a ZnCdSe/ZnCdMgSe QC structure based on a two-well active region.[12] The EL was measurable only at current densities higher than 1.2 kA/cm^2 and showed a rather large full width at half maximum (FWHM) of the EL spectrum (47 meV, ~20% of the peak emission energy at 80 K). The measured turn-on voltage was ~50% higher than the designed value. In this paper, we present ZnCdSe/ZnCdMgSe QC structures with 3 times higher luminescence efficiency, narrow EL FWHM (13% of the emission peak energy at 80 K) up to room temperature and as-designed turn-on voltage. This is achieved by facilitating improved electron transport through the injector and active regions and making the structures more robust to design and growth variations. Besides, waveguide designs suitable for II-VI epi-layers were used for better mode confinement in the active region and for lower waveguide loss.

We have developed two QC laser designs based on a "two-phonon" active region[13] at ~4.9 μm, i.e., design TP1 and its improved version TP2 shown in Fig. 1(a). Two states below the lower laser state in the active region were designed to depopulate electrons from the lower laser state ($\tau_l = 0.20$ ps). At the injection barrier, stronger coupling between the lowest injector state and the upper laser state (with an anti-crossing energy splitting of ~12 meV) was used to improve electron injection onto the latter.[14] Fig. 1(b) shows the band diagram of a structure based on the bound-to-continuum design[15] (named as BC) at an emission wavelength of 3.38 μm.

Compared with the previously demonstrated ZnCdSe/ZnCdMgSe QC structure,[7] these designs provide large tolerance to deviations in design parameters and growth, which is important considering the challenge in predicting material parameters and growing high quality nanometer-thick layers in this material system. For example, high resolution X-ray diffraction (XRD) measurements show that one grown structure based on design TP2 has wider barriers and wells (~12.5% on average). Despite of the large deviation between growth and design, the structure still provides efficient electron transport

[a)]Electronic mail: yuyao@seas.harvard.edu. Current address: School of Engineering and Applied Science, Harvard University, Cambridge, Massachusetts, 02138, USA.
[b)]Current Address: Physics Department, Cinvestav-IPN, Ave. IPN 2508, 07360 Mexico, Distrito Federal, Mexico.
[c)]Current address: Jet Propulsion Laboratory, California Institute of Technology, Pasadena, California 91109, USA.
[d)]Current address: Photonic Devices Inc., Raleigh, North Carolina 27606, USA.

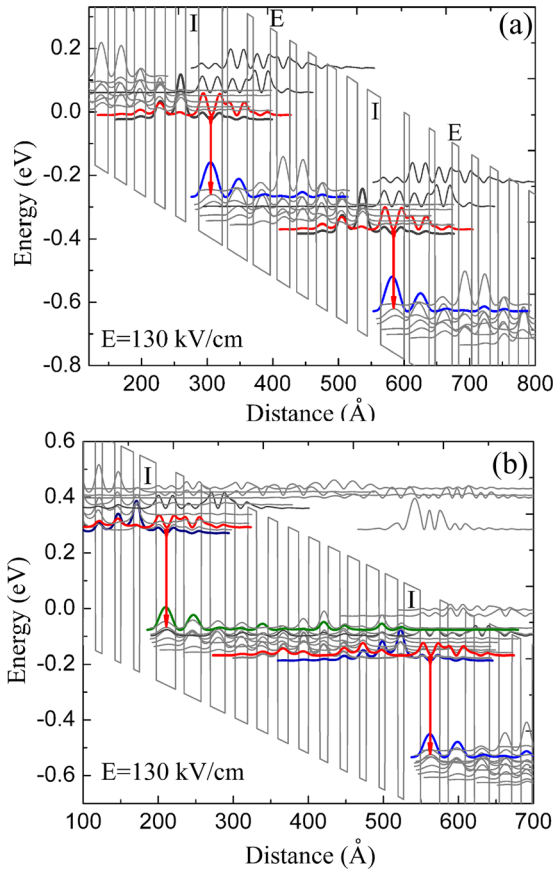

FIG. 1. (Color online) Conduction band diagram of a portion of two active regions and interleaving injectors and the moduli squared of the relevant wave functions for designs TP2 (a) and BC (b) at an electric field of 130 kV/cm. The layer sequence of one period in design TP2 (starting from the injection barrier, in angstrom) is **20**/36/**8**/30/**9**/26/**10**/20/**10**/18/**12**/17/**14**/16/**16**/15. Not shown is design TP1, which is very similar to design TP2, and has the following layer structure **20**/35/**7**/30/**8**/25/**10**/20/**7**/18/**11**/16/**15**/15/**18**/15. The layer sequence in design BC is **22**/26/**11**/23/**12**/20/**13**/17/**12**/15/**13**/14/**14**/13/**15**/11/**16**/10/**16**/9/**17**/8/**17**/8. $Zn_{0.20}Cd_{0.19}Mg_{0.61}Se$ barrier layers are in bold, $Zn_{0.43}Cd_{0.57}Se$ well layers are in normal font and the underlined layers are doped (Si, 3×10^{17} cm^{-3}).

through the injectors and sufficient coupling strength between the lowest injector state and the upper laser state (with an anticrossing energy splitting of 6.6 meV). The emission wavelength was shifted to 5.4 μm according to the simulation results.

Besides the gain medium, the waveguide structure is also a key factor in laser design. The goal of waveguide design is to maximize the mode confinement in the active region while minimizing the waveguide loss. Figure 2(a) shows the refractive indices of the epi-layers and InP substrate in a EL structure and the calculated light intensity distribution. Starting from the InP substrate, the epi-layer consists of a 250 nm InGaAs layer, a 500 nm ZnCdSe (Cl doped: 3×10^{17} cm^{-3}) bottom layer, 30 periods of active and injector regions, a 230 nm ZnCdSe top layer, and a 200 nm highly doped ZnCdSe (Cl doped: 5×10^{18} cm^{-3}) contact layer. This waveguide structure does not support a confined surface plasmonic mode but only a radiation mode, because the refractive index of the II-VI epi-layer (ZnCdSe: ~2.4, ZnCdMgSe: ~2.2) is smaller than that of the InP substrate. To circumvent this problem, highly doped quaternary ZnCdMgSe layers were introduced into both sides of the active core so as to support a dielectric waveguide mode in

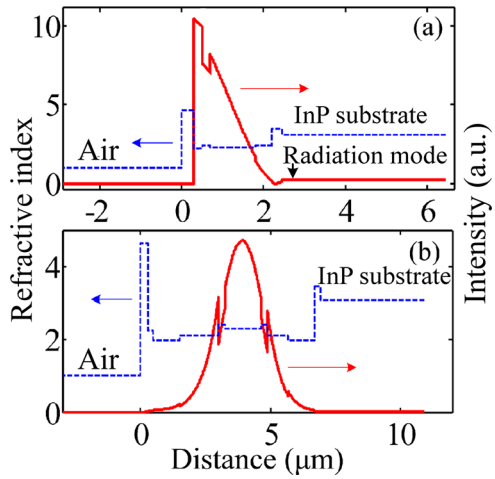

FIG. 2. (Color online) Refractive index profile of the waveguide structure (dashed line) and calculated waveguide mode intensity distribution (solid line) of (a) the plasmonic waveguide structure and (b) the dielectric waveguide structure.

the active region as shown in Fig. 2(b). This dielectric waveguide structure consists of, starting from the InP substrate, a 250 nm InGaAs buffer layer, a 90 Å ZnCdSe buffer layer, a 1.0 μm highly doped ZnCdMgSe (Cl doped: 5×10^{18} cm^{-3}) layer, a 0.8 μm ZnCdMgSe (Cl doped: 3×10^{17} cm^{-3}) bottom cladding layer, 30 periods of active and injector regions, a 1.5 μm ZnCdMgSe (Cl doped: 3×10^{17} cm^{-3}) top cladding layer, a 1.0 μm ZnCdMgSe (Cl doped: 5×10^{18} cm^{-3}) confinement layer and a final 200 nm highly doped ZnCdSe (Cl doped: 5×10^{18} cm^{-3}) contact layer. ZnCdSe/ZnCdMgSe grading layers are used between the bulk ZnCdMgSe and ZnCdSe layers as well as the active core to reduce the voltage drops over the barriers. Two structures with plasmonic waveguides were grown based on the designs BC and TP1 by molecular beam epitaxy (MBE). One structure with dielectric waveguide was grown based on design TP2. Electroluminescence structures were fabricated[12] in the form of circular (with a diameter of 400 μm and 200 μm) and rectangular mesas (100 and 200 μm wide).

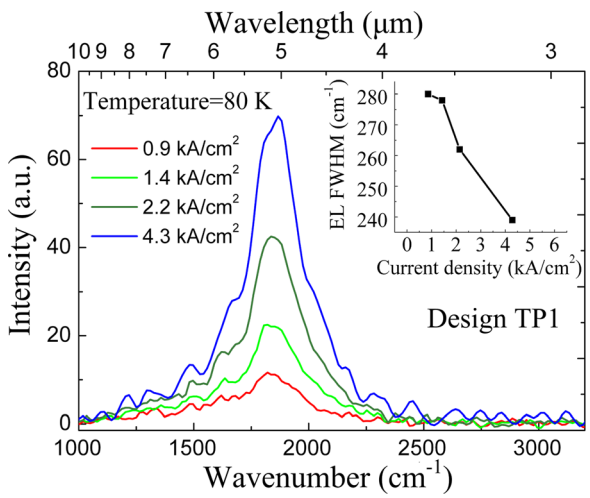

FIG. 3. (Color online) (a) Measured electroluminescence (EL) from design TP1 grown with a plasmonic waveguide structure at different injection current densities at a constant heat sink temperature of 80 K. The inset shows the EL full width at half maximum (FWHM) as a function of the current density.

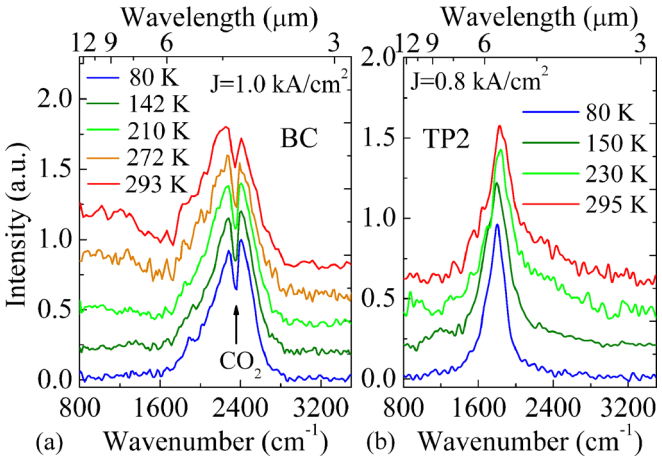

FIG. 4. (Color online) Measured EL at different heat sink temperatures of (a) design BC grown with a plasmonic waveguide structure and (b) design TP2 grown with a dielectric waveguide structure. All the EL data were taken with 80 kHz repetition rate and 200 ns pulse width.

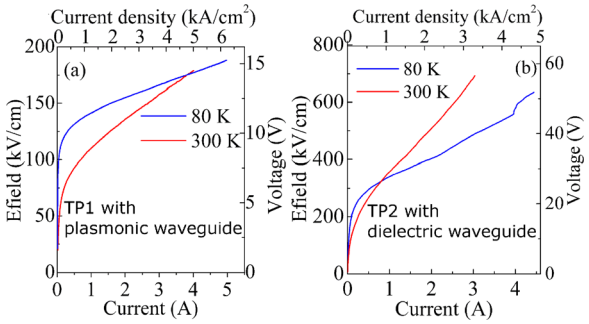

FIG. 5. (Color online) Measured current-voltage and electric field characteristics for (a) design TP1 (grown with plasmonic waveguide structure) and (b) design TP2 (grown with dielectric waveguide structure) at 80 K and 300 K. All data were taken with 5 kHz repetition rate and 100 ns pulse width.

Electroluminescence from half-cleaved mesas was measured at different temperatures and injection currents in pulsed mode (200 ns pulse width, 80 kHz) using a Fourier-transform infrared spectrometer (FTIR) with a cooled HgCdTe (MCT) detector. Fig. 3 shows the EL from a structure based on design TP1 with plasmonic waveguide at a heat sink temperature of 80 K. The inset shows the EL FWHM as a function of the current density. The EL width decreases as the injection current increases, exhibiting a smallest width of 30 meV, ~13% of the peak emission energy (~230 meV). The temperature dependence of the EL from design BC with plasmonic waveguide is shown in Fig. 4(a). Electroluminescence is measurable above a current density of 0.4 kA/cm^2 at 80 K, i.e., the luminescence efficiency is improved by at least 3 times compared to our previous designs.[7] The emission peak centered near 2380 cm^{-1} (~4.2 μm) is present over the full temperature range. The dips at 4.23 μm correspond to CO_2 absorption. A broader peak appears at temperatures above 200 K and becomes stronger and blue-shifted as temperature increase, which we attribute to thermal emission because of its un-polarized nature.

Temperature dependent EL from a dielectric waveguide structure based on design TP2 at a constant injection current density (0.8 kA/cm^2) is shown in Fig. 4(b). A single peak is maintained from 80 K up to room temperature, without observation of any background emission (thermal or other), which is an indication of improved EL intensity and luminescence efficiency. The EL FWHM is ~230 cm^{-1} (29 meV) at 80 K and increases to 300 cm^{-1} (37 meV) at room temperature. The EL peak is ~1805 cm^{-1} at 80 K and ~1828 cm^{-1} at room temperature. It is very close to the calculated emission energy (~1850 cm^{-1}) of the structure corrected according to the XRD results. The blue shift of the peak emission wavelength and the weak dependence of the EL FWHM as temperature increases are attributed to the fact that multiple transitions contribute to the EL.

The transport characteristics are also improved in the samples with plasmonic waveguide structures. From the current voltage (IV) curve of design TP1 shown in Fig. 5(a), we obtained a turn-on electric field of ~130 kV/cm, the same as the designed value. The differential resistance is about 1 Ω and 2 Ω at 80 K and 300 K, respectively. The major reasons for the improved transport characteristics are the stronger coupling between the injector states and the upper laser states as well as the large tolerance to the design and growth deviations. However, for the sample with dielectric waveguide structure, the IV curves show twice to three times higher turn-on voltage than the calculated value (~10 V), as shown in Fig. 5(b). We attribute the extra voltage drop to the ZnCdMgSe cladding layer because an "empty" waveguide structure without the active core also shows very high turn-on voltage and differential resistances.

In conclusion, we have demonstrated ZnCdSe/ZnCdMgSe QC structures with much improved QC designs that are more robust to design and growth variation. Electroluminescence from these structures shows more than 3 times higher luminescence efficiency, 40% narrower EL FWHM and as-designed turn-on voltage. A waveguide design was also demonstrated to support a dielectric waveguide mode and reduce the waveguide loss. Electroluminescence from such a structure shows a single narrow peak at the calculated emission wavelength, for all temperatures from 80 K to 300 K.

This work is supported in part by MIRTHE (NSF-ERC # EEC-0540832) and by CENSES (NSF # HRD-0833180). The authors would like to thank Prof. Jacob Khurgin for insightful discussions about the plasmonic waveguide structure.

[1]Q. J. Wang *et al.*, Appl. Phys. Lett. **94**, 011103 (2009).
[2]M. Razeghi, IEEE J. Sel. Top. Quantum Electron. **15**, 941 (2009).
[3]K. Fujita *et al.*, IEEE J. Quantum Electron. **46**, 683 (2010).
[4]Y. Yao *et al.*, Appl. Phys. Lett. **97**, 081115 (2010).
[5]M. P. Semtsiv *et al.*, Appl. Phys. Lett. **93**, 071109 (2008).
[6]N. Bandyopadhyay *et al.*, Appl. Phys. Lett. **97**, 131117 (2010).
[7]O. Cathabard *et al.*, Appl. Phys. Lett. **96**, 141110 (2010).
[8]J. P. Commin *et al.*, Appl. Phys. Lett. **97**, 031108 (2010).
[9]I. Vurgaftman *et al.*, New J. Phys. **11**, 125015 (2009).
[10]M. Sohel *et al.*, J. Vac. Sci. Technol. B **23**, 1209 (2005).
[11]O. Zakharov *et al.*, Phys. Rev. B **50**, 10780 (1994).
[12]K. J. Franz *et al.*, Appl. Phys. Lett. **92**, 121105 (2008).
[13]D. Hofstetter *et al.*, Appl. Phys. Lett. **78**, 396 (2001).
[14]Y. Yao *et al.*, Appl. Phys. Lett., **95**, 021105 (2009).
[15]J. Faist *et al.*, Appl. Phys. Lett. **78**, 147–149 (2001).